Accepted Manuscript:
Bollinger, D.L., J. Erickson, J.M. Bussey, and J.S. McCloy, "Process optimization of caustic scrubber and iodine-129 immobilization in sodalite-based waste forms," *MRS Advances*, 7, 110-116 (2022). https://doi.org/10.1557/s43580-022-00229-y

Process Optimization of Caustic Scrubber and Iodine-129 Immobilization in Sodalite-based Waste forms

David L. Bollinger, Jessica Erickson, John M. Bussey, John S. McCloy

Abstract

Caustic scrubbers are proposed to remove vaporized iodine from nuclear fuel reprocessing plants. Resulting caustic slurries of radioactive iodine (^{129}I) and other anions can be captured and immobilized into the cage structures of sodalite-type minerals. Here, mixed anion sodalites were hydrothermally synthesized from a simulated caustic scrubber solution containing hydroxide/water, carbonate, chlorine, bromine, iodine, nitrate, and nitrite ions with added kaolinite. Experiments were conducted with twenty-five different sets of process conditions. Resulting powders were characterized by quantitative X-ray diffraction (XRD) and multi-functional thermal analysis, including gravimetry, calorimetry, and mass spectrometry. Using statistical analysis, process variables were tailored to maximize conversion of kaolinite into cage silicates, immobilize caustic scrubber anions, and minimize amorphous content. Chemical analysis showed the incorporation of all the targeted ions into the solids. Detailed investigation of a batch characterized after washing (creating secondary waste) and one without washing but subsequent calcination is given. This work contributes to defining the constraints required for subsequent consolidation process steps of the waste form to avoid volatilization.

Introduction

A significant challenge in nuclear waste management is the safe, long-term disposal of iodine-129. Issues with the disposal of ^{129}I include high groundwater mobility, a long half-life (15.7 million years), and its incompatibility with typical vitrification technologies [1]. Caustic Scrubbers (CS) are a proposed method to remove gaseous iodine from envisioned spent nuclear fuel (SNF) reprocessing plants in the United States [2,3]. In the early steps of such a plant, iodine (^{129}I) and other gaseous fission products including ^{3}H, ^{14}C, and ^{85}Kr are released during dissolution of the SNF. Current European reprocessing plants release ^{129}I vapor directly into the environment, a solution that is unsustainable in the long term [1]. With a caustic scrubber process, the gaseous iodine can be captured with a caustic scrubber tower in concert with an Ag-embedded solid sorbent bed as a final removal 'polishing' step [4].

One way to dispose of the resulting caustic slurry waste stream of ^{129}I, other halogens, and oxyanions, entails immobilizing them into cage-type aluminosilicate minerals. The cage structures [5] of sodalite (SOD) – e.g., $Na_8Al_6Si_6O_{24}I_2$ – and cancrinite (CAN) – e.g., $Na_8Al_6Si_6O_{24}(OH)_2 \cdot 2H_2O$ – can incorporate ^{129}I and a variety of other anions with a -1 or -2 charge. The general formula of both SOD and CAN is $Na_8(AlSiO_4)_6X_2$, where X = -1 anion. Furthermore, sodalites and cancrinites can be pressed with a suitable glass binder and sintered at low temperatures, to ensure retention of iodine, into a vitrified waste form for long term storage. Previous work has developed processes for hydrothermal and aqueous synthesis of sodalites and cancrinites [6–13].

Synthesis of SOD, CAN, and other porous aluminosilicates (e.g., zeolites) has previously been extensively studied for radioisotope immobilization [6–8,11,13–20]. Various synthesis routes have been proposed for providing the aluminum and silicon for producing sodalite, most commonly kaolinite [6,8,9], metakaolin [6,8,21], $NaAlO_2$ + colloidal SiO_2 or Na_2SiO_3 [6,8,22], aluminum-isopropoxide + tetraethyl-orthosilicate (TEOS) [23,24], or zeolite 4A [8,10,11,25]. The reactions are typically in an aqueous (uncapped) or hydrothermal (mildly pressurized) environment in a solution of water plus NaOH and any other Na-anion salt (in this case, carbonate, nitrate, nitrite, chloride, bromide, and iodide) as desired. In the current study, we chose to use kaolinite (KAO) as the precursor; a previous direct comparison [8] showed slightly higher conversion with zeolite 4A but required high excess NaOH, while KAO still resulted in a high conversion to iodosodalite in the presence of water without excess NaOH in a later study [6].

Here, experimental parameters were varied to maximize conversion of a KAO precursor into SOD and CAN products, while incorporating caustic scrubber anions (i.e., hydroxide, chloride, iodide, bromide, nitrate, nitrite, carbonate) and minimizing the amorphous content. Furthermore, in an industrial setting, optimizing process conditions for SOD and CAN synthesis can improve mixed-anion SOD and CAN product properties. Additionally, optimization can lead to reduction in energy demand, water use, and waste form mass, lowering system costs and environmental impacts. This work is the first step at optimization of the process for iodine immobilization into the synthetic ceramic powders and provides the basis for ongoing work on immobilizing caustic scrubber solution into aluminosilicates.

Materials & Methods

The assumed approximate composition of the caustic scrubber from a SNF waste stream is [26]: NaOH (0.2 M), NaI (0.03 M), NaCl + NaBr (0.1 M), Na_2CO_3 (0.6 M), $NaNO_3$ (0.03 M), $NaNO_2$ (0.06 M). The -1 and -2 charge anions can be incorporated into SOD in different amounts: as two anions of -1 charge or one anion of -2 charge (see Eq. 1) [6,15,16]. For example,

$Na_8(AlSiO_4)_6A_2$ or $Na_8(AlSiO_4)_6B$ if A = -1 anion, B = -2 anion. As in Chong et al [16], excess NaOH was avoided to maximize the uptake of non-OH anions into the sodalite cage and minimize residual NaOH. Because of the ubiquitous presence of hydroxide and water, which both go into the cage of sodalite [24,27], we did not supply excess Al+Si in the form of the KAO precursor. In our experience, additional KAO results in more hydrosodalite products (containing OH^- and water), instead of the desired halide sodalite products [9]. The synthesis procedure essentially consists of mixing caustic scrubber solution with a stoichiometric amount of kaolinite (KAO).

***Sodalite Synthesis*:** $3KAO + 6NaOH + 2\left(NaA + \frac{1}{2}Na_2B\right) \rightarrow SOD + 9H_2O$ Equation 1

e.g., $3[Al_2Si_2O_5(OH)_4] + 6NaOH_{(aq)} + 2NaI_{(aq)} \rightarrow Na_8(AlSiO_4)_6(I)_2 + 9H_2O$

$SOD \equiv Na_8(AlSiO_4)_6(A)_2 \ or \ Na_8(AlSiO_4)_6B;\ A{:}\ OH^{-1}, Cl^{-1}, I^{-1},\ Br^{-1}, NO_3{}^{-}, NO_2{}^{-};\ B{:}\ CO_3{}^{2-}$

Aqueous and hydrothermal procedures were employed to synthesize a mixed sodalite solid material from kaolinite and a simulant caustic scrubber solution, containing non-radioactive iodine. The ideal stoichiometry is 2 mol NaOH to 1 mol KAO as described in Eq. 1. Various stoichiometries were synthesized to examine alternate products and process sensitivity. The reactions occurred when powdered KAO reacted in suspension with caustic solution and re-formed as SOD and CAN minerals.

To investigate ideal conversion to SOD, time, temperature, and reaction vessel type were varied. Sample batches were reacted for durations between one hour and one month. Three synthesis methods were used. 1) In the autoclave method, the reaction mixture was transferred from a stirred beaker to a PTFE-lined Parr autoclave and heated in an oven at 90°C, 120°C, or 150°C. 2) In the stirred autoclave method, the reaction mixture was heated on a hotplate, potentially creating more thorough mixing to increase conversion of KAO to SOD. 3) In the third method, only feasible below 90°C, the reaction mixture was heated and stirred in a loosely capped jar on a hotplate. A summary of the details of the process parameters for each batch is provided in Table S-1.

After the desired aging time, a subset of the batches were washed with deionized water in a centrifuge to remove residual reactants, while others were first dried to drive the reaction to completion (Eq. 1), and then washed. Some samples were calcined at 550°C after drying and aging with no washing step, to remove chemically bonded water and to test for iodine volatilization. Removing the washing step eliminates an additional wastewater stream (secondary waste) and significantly reduces water consumption, both primary objectives in a scaled-up process. All batches were dried at 105°C to remove sorbed water but not chemically bound water of hydration.

For characterization, samples were crushed and mixed with a mortar and pestle to ensure homogeneity. Powder XRD spectra were collected for each sample with a Panalytical X'Pert Pro diffractometer using CuK_{α} radiation (λ = 1.5418740 Å). Data was collected in 0.0501° step increments at 5.080 s per step over a 2θ range of 5-90°. In order to improve signal to noise ratio, 5 scans were summed. Diffraction patterns were analyzed with HighScore Plus (Malvern Panalytical) software to identify phases.

Quantitative analysis included Rietveld fitting with an internal standard (20 wt% CaF_2 or corundum Al_2O_3) enabling calculation of amorphous fraction. Contents of SOD, CAN, residual KAO, and amorphous material were of particular focus. Phase composition data was analyzed with JMP software (SAS, Inc.), which allowed statistical exploration and data visualization to elucidate relationships between process variables (i.e., time, temperature, reactor vessel type, and phase composition).

Thermogravimetric methods were employed to measure temperature dependent heat and mass fluxes to compare with single phase standards – i.e., iodo-SOD, hydro-SOD, carbonate-CAN (see Supplementary information) [24,28]. Preliminary thermal analysis data was collected on a TA Instruments SDT-Q600 thermal analyzer (i.e., for Thermogravimetric – Differential Thermal Analysis, TG-DTA). For TG-DTA, 13-18 mg samples were heated in alumina crucibles to 1250°C at a constant rate of 10°C/min with 100 mL/min of N_2 gas flowing across the sample. More accurate heat flux measurements and the identity of gas volatilization during phase transitions (i.e., material decomposition) was subsequently collected with a Netzsch instrument STA 449 F3 Jupiter® STA-QMS 403 D Aëolos® quadrupole mass spectrometer coupling (i.e., for Thermogravimetric – Differential Scanning Calorimetry – Mass Spectrometry, TG-DSC-MS).

Chemical analysis of the presence of anions in the CS product and standards was determined by several methods. First, in the TG-DSC-MS above, ion current was measured for H_2O and CO_2 off-gas. Second, energy dispersive spectroscopy (EDS) was used in a scanning electron microscope (SEM) to look for halides. Finally, commercial chemical analysis (Gilbraith Laboratories, Knoxville, TN, USA) was performed for nitrate, nitrite, chloride, and bromide by ion chromatography, iodide by an ion selective electrode method, and carbonate as carbon by a coulometric method.

Results and Discussion

X-ray diffraction

XRD data allows for many phase composition observations between samples. It was determined that the converted caustic scrubber solids were primarily comprised of SOD and CAN minerals and a fraction of amorphous content, as seen in Fig. 1. Numerical phase fraction data is shown in Table S-1, along with goodness-of-fit parameters. Example Rietveld fits are given in Fig. S-13 through Fig. S-16). Given the difficulty and inconsistency in distinguishing various sodalites (with single or mixed anions in the beta cage, see Fig. S-17), only the total sodalite fraction from XRD was considered.

Samples with 2:1 NaOH to KAO ratio exhibited more complete KAO to SOD conversion, as was expected from stoichiometry. More complete KAO to SOD conversion occurred at longer aging times (> 3 d) and at higher temperatures (≥ 90°C). More complete conversion at higher temperatures was enabled with autoclave reactors. At the lowest temperature (60°C) and conversion times (1 h to 3 d), a large amount of KAO remained, although some amorphous phase still formed (Fig. 2). Evidence of residual KAO is also confirmed via thermal analysis (Fig. S-4).

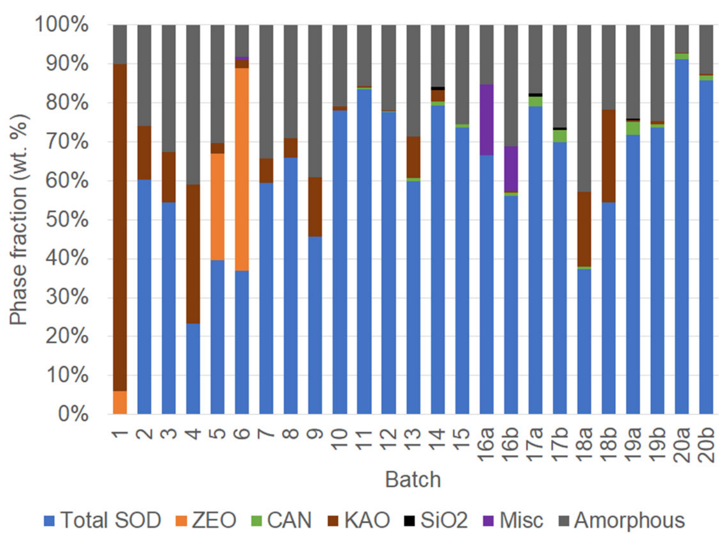

Figure 1: Phase composition of each synthesized batch. Blue is combined SOD phases, brown is KAO, orange is zeolite, green is cancrinite, grey is amorphous, black is silica, and purple contains miscellaneous additional phases (Misc.). Batches 16a & b had significant quantities of residual $NaCO_3$ and NaCl.

The bubble plot in Fig. 2 allows visualization of the relationships between phase composition and process variables revealing a clear relationship between KAO conversion to SOD, and ultimately showing that this process was more complete at higher temperatures (indicated by color). Amorphous content in the samples is indicated by bubble size, and samples 5 and 6 are outliers because of their high zeolite (ZEO) content, here identified by XRD as zeolite Na-P [29]. In a previous study [30], this phase was shown to be an intermediate one between an amorphous phase and SOD which eventually ripened into CAN. Other relationships are shown in Fig. S-1, Fig. S-2, and Fig. S-3.

Greater temperatures and aging times converted more of precursor KAO into product SOD, incorporating caustic scrubber anions from the slurry (Fig. 2). Minor amounts of CAN were formed in some samples. Autoclave reactors allowed for higher temperatures associated with more complete conversion. Most samples were washed in post processing steps, although there was little evidence in XRD of soluble salts in the batch 17 unwashed products (17b). Moreover, sample 17a was calcined, while 17b was left uncalcined; this calcination at 550°C for 1 h reduced the amorphous content of 17b by about 9% with respect to 17a (Table S-1).

During hydrothermal sodalite synthesis, zeolites can form as intermediates [7,10,22,31–33], and were confirmed in TG-DTA in batches 1, 5, and 6 (Fig. S-6). Zeolite appears to be an ephemeral step in KAO to SOD conversion though, as it was only seen in these three samples. Another hypothesized KAO → SOD pathway involves partial dissolution of KAO into amorphous material followed by SOD recrystallization. This is supported by the XRD evidence that all samples contain amorphous content (Table S-1, Fig. 1). No samples showed complete conversion from KAO to 100% caged silicates, i.e., SOD + CAN (Fig. 2, Fig. S-3).

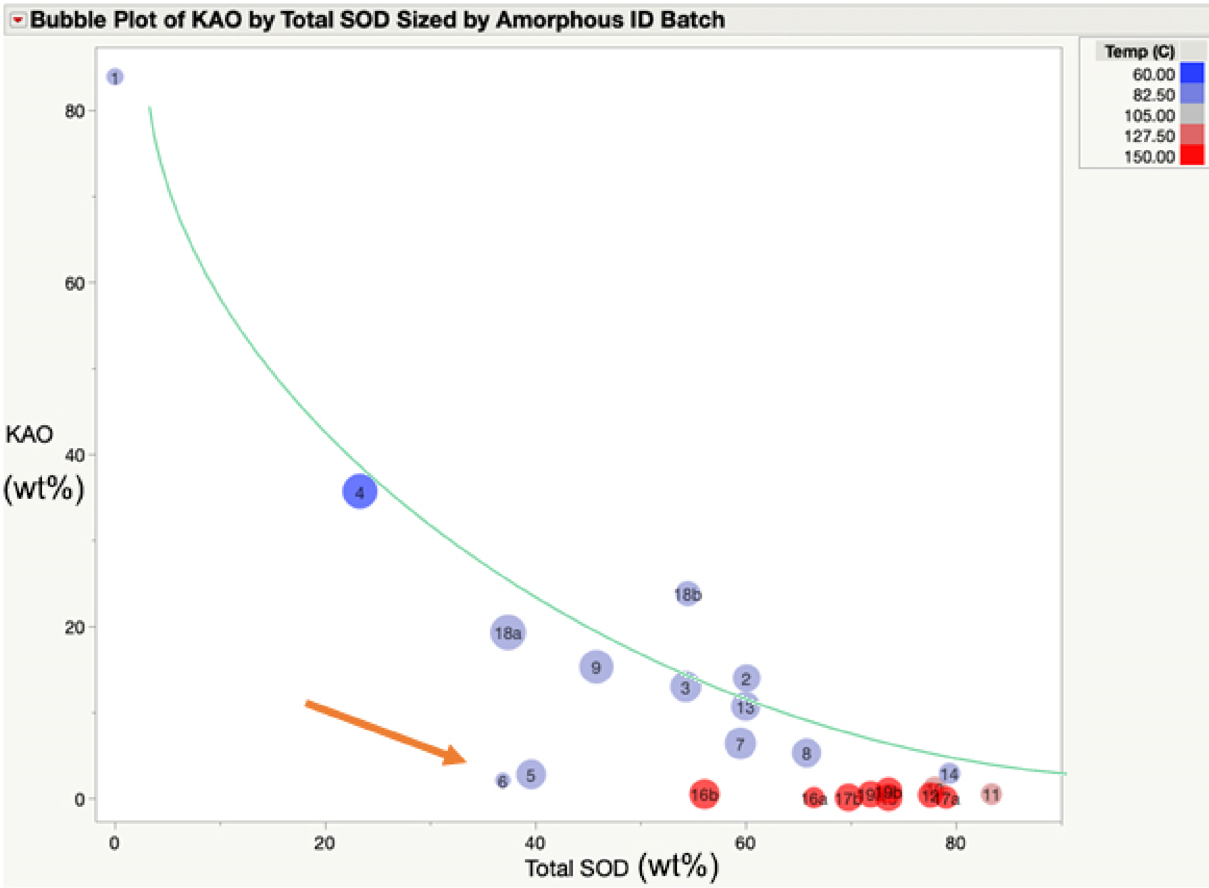

Figure 2: Relationship between residual KAO (y-axis) and synthesized SOD (x-axis), in weight percent, as determined by XRD Rietveld refinement. Batch numbers are shown in the bubbles, and a green trendline is shown as a guide to the eye. Bubbles show that higher synthesis temperatures (redder) produced more sodalite and consumed more kaolinite. Samples 5 & 6 (orange arrow) are outliers on the KAO to SOD relationship because of their high ZEO content, a reaction intermediary between KAO and SOD. Circle size represents amorphous content, larger-higher, smaller-lower.

Thermal analysis

TG-DSC-MS and TG-DTA measurements allowed for an examination of the thermal decomposition of the synthesized materials. At temperatures above 700°C, SOD decomposes into carnegieite (CAR) and subsequently to nepheline near 900°C. First, the SOD cage breaks down, releasing the cage anion as a volatilized salt and rearranges into the channeled structure of CAR as in Eq. 2. Then with additional heating, the CAR can transform into nepheline [34–36]. These transitions are shown in thermal analysis (Fig. S-5).

$$Na_8(AlSiO_4)_6X_{2\,(s)} \rightarrow 6NaAlSiO_{4\,(s)} + 2NaX_{(g)} \qquad \text{Equation 2}$$

Shown in Fig. 3, TG-DSC-MS identifies a complex event slightly above 800°C noted by a mass loss (TG), an exothermic peak within an endothermic peak (differential scanning calorimetry, DSC), and a spike in CO_2 release (mass spectrometry, MS). CO_2 is the primary cage anion measurable with this TG-DSC-MS equipment, as halides are believed to deposit on the transfer tube despite the tube being heated.

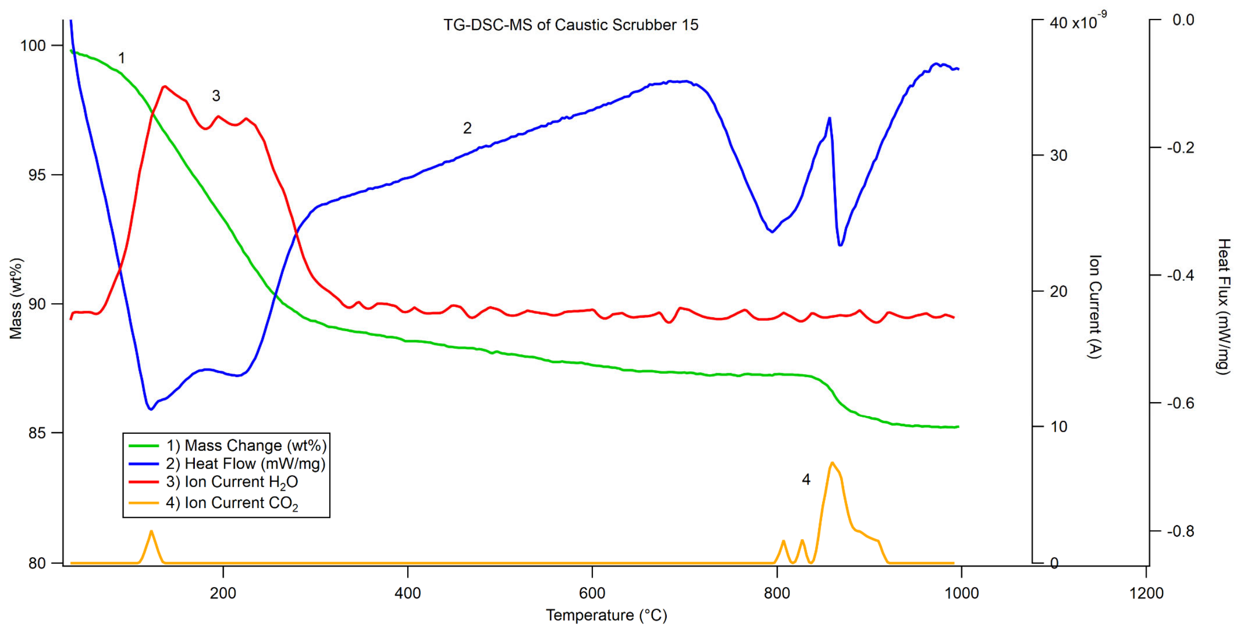

Figure 3: TG-DSC-MS spectra from Caustic Scrubber sample 15. Shown is 1) mass change (green), 2) heat flow (blue), 3) ion current H_2O (red), 4) ion current CO_2 (orange).

Another significant feature noted in TG-DSC-MS is water loss that occurs up to ~400°C in temperature. At ≈100°C, water adsorbed from ambient air is driven out of all samples. Then, at higher temperatures, waters of hydration in SOD or CAN cages are driven off. These two features were measured in MS (Fig. 3) and have distinct endothermic peaks for the maximum water losses.

As evidenced by the TG-DSC-MS investigation of CS 15 (Fig. 3), we hypothesize that the broader endothermic peak (~700-975°C) that encompasses a sharp exothermic one (795-870°C) from CO_2 evolution (evidenced by MS) is related to a phase change from SOD to CAR. As the SOD is heated, carbonate becomes excited in its cage structure but is unable to exit. At higher temperatures when the cage starts to break down, the CO_2 is lost rapidly and exothermically, and then the cage structure finishes relaxing and breaking down as the SOD becomes CAR. It is also possible that this phase change is two subsequent endotherms: SOD to CAR, then CAR to nepheline (NEP). The Gibbs free energy (ΔG) of SOD is much more negative than the ΔG of CAR, indicating that the SOD → CAR transition is endothermic [37]. To help elucidate this transition, hot stage in situ X-ray diffraction (XRD) is planned in future work.

In sample CS 17a (calcined) (Fig. S-8), a stepped down endothermic transition between 690°C and 1000°C was observed, suggesting a transition pathway of SOD → CAR → NEP. Carbon dioxide evolution peaks at 855°C (MS ion current, envelope ~815-900°C) with a 3% loss in weight as a result. Both samples lose water of hydration at low temperatures (i.e., OH, H_3O_2, and/or water in the SOD cages [24]), up to temperatures around 300°C. CS 15 loses a small amount of CO_2, centered on 122°C, which coincides with the loss of hydration water and its related endotherm. This CO_2 is possibly associated with water as a loosely bound bicarbonate, but it is not seen in MS data on CS 17a.

Similar heat and mass fluxes were calculated from TG-DTA as in TG-DSC-MS, although TG-DTA results were less definitive. TG-DTA identified similar SOD to CAR transitions across a range of synthesized mixed SODs and standards and showed the release of hydration water at temperatures < 200°C (Fig. S-5). TG-DTA of different SOD standards indicated that the temperature of the SOD to CAR transition can shift due to different SOD cage anions (Fig. S-6). Transitions seen in both TG-DTA and TG-DSC-MS were identified, including SOD decomposition to CAR, KAO transition to metakaolinite to mullite, zeolite, CAN decomposition, adsorbed and hydrated water losses (Fig. S-4, Fig. S-6).

Moreover, TG-DSC-MS (Fig. 3, Fig. S-8) helped elucidate the SOD to CAR transition, identified between 700°C and 900°C. Here, the SOD cage decomposes, releasing the cage anions (including presumably I^-), a key factor in iodine retention. TG-DTA revealed that the identity of the cage anion leads to a variable temperature of decomposition.

While the TG-DSC-MS instrument detected water and carbon dioxide evolution from the CS samples, it could not detect nitrogen oxides because its carrier gas was nitrogen. Further, no halides (chlorine, bromine, iodine) were detected. As previously stated, this is likely due to condensation in the transfer line between the TG-DSC and MS instrument units. Even with an iodosodalite standard, no iodine signal was observed in the TG-DSC-MS (Fig. S-7).

Chemical analysis

To confirm the original capture of the various anions in the mixed phase CS materials and the standards, several methods were employed. As stated in the previous section, water-related species (OH, H_3O_2, H_2O) can be assessed by thermal analysis methods and MS. Carbonate can be seen by MS as well as chemical analysis. In the coulometric chemical analysis, carbonate was observed in the CS 15 and CS 17a solid samples, as well as in the 'hydro'-SOD standard, the cancrinite standard, and the iodo-SOD standard. Its presence in iodo-SOD is likely due to CO_2 from the air dissolving into the water of the hydrothermal vessel. EDS was unable to detect the presence of iodine in the measured CS samples (Fig. S-10) but did so in the iodo-SOD standard (Fig. S-9). Chemical analysis, however, showed iodine in all the CS samples as well as iodo-SOD, and in the CS samples approximately 1/3 of the targeted iodine was present in the CS solid. Lower amounts of the other halides, nitrate, and nitrate were apparently captured, though some interferences in the ion chromatography technique used cannot be ruled out. The calcined sample (CS 17a) showed higher incorporation of chloride and bromide than the washed sample (CS 15) hinting at further incorporation of these anions into non-soluble phases during a calcine step. The chemical analysis data is summarized in Table S-3, Fig. S-11, and Fig. S-12.

We have shown here that a mixture of sodalite endmembers have been successfully synthesized from a caustic, mixed anion waste stream, demonstrating the potential for sodalites to immobilize caustic scrubber slurry in potential SNF reprocessing plants. XRD characterization alone cannot distinguish between most sodalite endmembers, especially when mixed phases are present, and cannot provide information about composition of amorphous phases. Thermal analysis methods provide some additional insight, especially indicating the importance of both water-related species and carbonate in these mixed phases. Further studies are in progress to ascertain the nature of the mixed sodalites (nuclear magnetic resonance, infrared spectroscopy), the detailed phase transformations on heating (hot-stage XRD), and the cage site preferences for anions in the presence of all the CS solution species. Results from this work also provide additional insight to the ongoing design of CS consolidation efforts by glass binding, sintering, and hot isostatic pressing of these waste forms, which will be reported in forthcoming work.

Summary

In this work, a simulated caustic scrubber solution containing sodium hydroxide and dissolved ions (nitrate, nitrite, carbonate, chloride, bromide, iodide) were synthesized by aqueous and hydrothermal methods and converted to aluminosilicates, primarily sodalite, using kaolinite for the aluminum and silicon. Given the propensity for sodalite to accommodate many anions and their coincident, overlapping XRD patterns, thermal and chemical analyses were used to help assess the materials. Water/hydroxide species and carbonate were confirmed using mass spectrometry, but halides and nitrogen compounds were not observed. However, these species were confirmed to be present in the solids by chemical analyses. These low temperature processes are promising for conversion of caustic scrubber solution to durable aluminosilicates with anion cages. Through these studies, temperature constraints were obtained for subsequent processing, in which these aluminosilicate powders will be consolidated into monoliths using glass bonding and sintering or hot isostatic press thermal treatment.

Acknowledgements

This work was supported by the US Department of Energy – Nuclear Energy University Program (NEUP), DE-NE0008964. The authors thank Saehwa Chong and colleagues for supplying the standards of iodo-SOD, Zeolite-P, and carbonate-CAN standards. Additionally, we thank Xianghui Zhang and Di Wu for TG-DSC-MS measurements and help with interpretation. Finally, we thank Brian Riley and Dan Gregg for helpful discussions.

Data Availability

Additional data supporting the findings of this study are available from the corresponding author upon reasonable request.

Compliance with ethical standards

Conflict of Interest: The authors declare no known conflicts of interest.

References

[1] R. Michel, A. Daraoui, M. Gorny, D. Jakob, R. Sachse, L. Tosch, H. Nies, I. Goroncy, J. Herrmann, H.-A. Synal, M. Stocker, V. Alfimov, Iodine-129 and iodine-127 in European seawaters and in precipitation from Northern Germany, Science of The Total Environment. 419 (2012) 151–169. https://doi.org/10.1016/j.scitotenv.2012.01.009.

[2] R.T. Jubin, Design and Test Plan for an Integrated Iodine Scrubber and Polishing Bed System, 2017. https://doi.org/10.2172/1426576.

[3] B.J. Riley, J.D. Vienna, D.M. Strachan, J.S. McCloy, J.L. Jerden, Materials and processes for the effective capture and immobilization of radioiodine: A review, Journal of Nuclear Materials. 470 (2016) 307–326. https://doi.org/10.1016/j.jnucmat.2015.11.038.

[4] S. Chong, B.J. Riley, J.A. Peterson, M.J. Olszta, Z.J. Nelson, Gaseous Iodine Sorbents: A Comparison between Ag-Loaded Aerogel and Xerogel Scaffolds, ACS Appl. Mater. Interfaces. 12 (2020) 26127–26136. https://doi.org/10.1021/acsami.0c02396.

[5] N.V. Chukanov, S.M. Aksenov, R.K. Rastsvetaeva, Structural chemistry, IR spectroscopy, properties, and genesis of natural and synthetic microporous cancrinite- and sodalite-related materials: A review, Microporous and Mesoporous Materials. 323 (2021) 111098. https://doi.org/10.1016/j.micromeso.2021.111098.

[6] J. Nam, S. Chong, B.J. Riley, J.S. McCloy, Iodosodalite Waste Forms from Low-Temperature Aqueous Process, MRS Adv. 3 (2018) 1093–1103. https://doi.org/10.1557/adv.2018.225.

[7] S. Chong, J. Peterson, J. Nam, B. Riley, J. McCloy, Synthesis and characterization of iodosodalite, J Am Ceram Soc. 100 (2017) 2273–2284. https://doi.org/10.1111/jace.14772.

[8] S. Chong, J.A. Peterson, B.J. Riley, D. Tabada, D. Wall, C.L. Corkhill, J.S. McCloy, Glass-bonded iodosodalite waste form for immobilization of 129I, Journal of Nuclear Materials. 504 (2018) 109–121. https://doi.org/10.1016/j.jnucmat.2018.03.033.

[9] D.L. Bollinger, J. Erickson, N. Stone-Weiss, A.J. Lere-Adams, S. Karcher, I.D. Akin, J.S. McCloy, Structure of amorphous aluminosilicates obtained from mineral transformation: potential path for partial remediation of alkaline bauxite residues, Environmental Advances. (2021) 100136. https://doi.org/10.1016/j.envadv.2021.100136.

[10] J.O. Dickson, J.B. Harsh, W.W. Lukens, E.M. Pierce, Perrhenate incorporation into binary mixed sodalites: The role of anion size and implications for technetium-99 sequestration, Chemical Geology. 395 (2015) 138–143. https://doi.org/10.1016/j.chemgeo.2014.12.009.

[11] K. Lilova, E.M. Pierce, L. Wu, A.M. Jubb, T. Subramani, A. Navrotsky, Energetics of Salt-Bearing Sodalites, $Na_8Al_6Si_6O_{24}X_2$ (X = SO_4, ReO_4, Cl, I): A Treatment Option for Pertechnetate-Enriched Nuclear Waste Streams, ACS Earth Space Chem. 4 (2020) 2153–2161. https://doi.org/10.1021/acsearthspacechem.0c00244.

[12] B.J. Riley, J.A. Peterson, S. Chong, J.D. Vienna, Influence of ion site occupancies on the unit cell parameters, specific volumes, and densities of $M_8(AlSiO_4)_6X_2$ sodalites where M = Li, Na, K, Rb, and Ag and X = Cl, Br, and I, Phys Chem Minerals. 48 (2021) 3. https://doi.org/10.1007/s00269-020-01124-4.

[13] J.J. Neeway, N.P. Qafoku, B.D. Williams, M.M.V. Snyder, C.F. Brown, E.M. Pierce, Evidence of technetium and iodine release from a sodalite-bearing ceramic waste form, Applied Geochemistry. 66 (2016) 210–218. https://doi.org/10.1016/j.apgeochem.2015.12.017.

[14] E.R. Maddrell, E.R. Vance, D.J. Gregg, Capture of iodine from the vapour phase and immobilisation as sodalite, Journal of Nuclear Materials. 467 (2015) 271–279. https://doi.org/10.1016/j.jnucmat.2015.09.038.

[15] E. Maddrell, A. Gandy, M. Stennett, The durability of iodide sodalite, Journal of Nuclear Materials. 449 (2014) 168–172. https://doi.org/10.1016/j.jnucmat.2014.03.016.

[16] S. Chong, B.J. Riley, R.M. Asmussen, A.R. Lawter, S.H. Bruffey, J. Nam, J.S. McCloy, J.V. Crum, Iodosodalite synthesis with hot isostatic pressing of precursors produced from aqueous and hydrothermal processes, Journal of Nuclear Materials. 538 (2020) 152222. https://doi.org/10.1016/j.jnucmat.2020.152222.

[17] E.R. Maddrell, E.R. Vance, C. Grant, Z. Aly, A. Stopic, T. Palmer, J. Harrison, D.J. Gregg, Silver iodide sodalite – Wasteform / HIP canister interactions and aqueous durability, Journal of Nuclear Materials. 517 (2019) 71–79. https://doi.org/10.1016/j.jnucmat.2019.02.002.

[18] E.R. Vance, D.J. Gregg, C. Grant, A. Stopic, E.R. Maddrell, Silver iodide sodalite for 129I immobilisation, Journal of Nuclear Materials. 480 (2016) 177–181. https://doi.org/10.1016/j.jnucmat.2016.08.013.

[19] M. ul Hassan, S. Venkatesan, H.J. Ryu, Non-volatile immobilization of iodine by the cold-sintering of iodosodalite, Journal of Hazardous Materials. 386 (2020) 121646. https://doi.org/10.1016/j.jhazmat.2019.121646.

[20] S. Venkatesan, M. ul Hassan, H.J. Ryu, Adsorption and immobilization of radioactive ionic-corrosion-products using magnetic hydroxyapatite and cold-sintering for nuclear waste management applications, Journal of Nuclear Materials. 514 (2019) 40–49. https://doi.org/10.1016/j.jnucmat.2018.11.026.

[21] H. Trill, H. Eckert, V.I. Srdanov, Mixed Halide Sodalite Solid Solution Systems. Hydrothermal Synthesis and Structural Characterization by Solid State NMR, J. Phys. Chem. B. 107 (2003) 8779–8788. https://doi.org/10.1021/jp0224618.

[22] Y. Deng, M. Flury, J.B. Harsh, A.R. Felmy, O. Qafoku, Cancrinite and sodalite formation in the presence of cesium, potassium, magnesium, calcium and strontium in Hanford tank waste simulants, Applied Geochemistry. 21 (2006) 2049–2063. https://doi.org/10.1016/j.apgeochem.2006.06.019.

[23] H. Trill, H. Eckert, V.I. Srdanov, Topotactic Transformations of Sodalite Cages: Synthesis and NMR Study of Mixed Salt-Free and Salt-Bearing Sodalites, J. Am. Chem. Soc. 124 (2002) 8361–8370. https://doi.org/10.1021/ja012765s.

[24] E.C. Moloy, Q. Liu, A. Navrotsky, Formation and hydration enthalpies of the hydrosodalite family of materials, Microporous and Mesoporous Materials. 88 (2006) 283–292. https://doi.org/10.1016/j.micromeso.2005.09.020.
[25] E.M. Pierce, K. Lilova, D.M. Missimer, W.W. Lukens, L. Wu, J. Fitts, C. Rawn, A. Huq, D.N. Leonard, J.R. Eskelsen, B. F. Woodfield, C.M. Jantzen, A. Navrotsky, Structure and Thermochemistry of Perrhenate Sodalite and Mixed Guest Perrhenate/Pertechnetate Sodalite, Environ. Sci. Technol. 51 (2017) 997–1006. https://doi.org/10.1021/acs.est.6b01879.
[26] R.T. Jubin, email communication, Composition of caustic scrub solution, (2019).
[27] G. Engelhardt, J. Felsche, P. Sieger, The hydrosodalite system $Na_{6+x}[SiAlO_4]_6(OH)_x{\cdot}nH_2O$: formation, phase composition, and de- and rehydration studied by 1H, 23Na, and 29Si MAS-NMR spectroscopy in tandem with thermal analysis, x-ray diffraction, and IR spectroscopy, J. Am. Chem. Soc. 114 (1992) 1173–1182. https://doi.org/10.1021/ja00030a008.
[28] J. Schliesser, K. Lilova, E.M. Pierce, L. Wu, D.M. Missimer, B.F. Woodfield, A. Navrotsky, Low temperature heat capacity and thermodynamic functions of anion bearing sodalites $Na_8Al_6Si_6O_{24}X_2$ (X = SO_4, ReO_4, Cl, I), The Journal of Chemical Thermodynamics. 114 (2017) 14–24. https://doi.org/10.1016/j.jct.2017.05.035.
[29] U. Håkansson, L. Fälth, S. Hansen, Structure of a high-silica variety of zeolite Na-P, Acta Crystallogr C Cryst Struct Commun. 46 (1990) 1363–1364. https://doi.org/10.1107/S0108270189013260.
[30] N.D. Pahlevi, B. Guo, K. Sasaki, Immobilization of selenate in cancrinite using a hydrothermal method, Ceramics International. 44 (2018) 8635–8642. https://doi.org/10.1016/j.ceramint.2018.02.083.
[31] C. Belviso, F. Cavalcante, G. Niceforo, A. Lettino, Sodalite, faujasite and A-type zeolite from 2:1dioctahedral and 2:1:1 trioctahedral clay minerals. A singular review of synthesis methods through laboratory trials at a low incubation temperature, Powder Technology. 320 (2017) 483–497. https://doi.org/10.1016/j.powtec.2017.07.039.
[32] L. Ding, H. Yang, P. Rahimi, O. Omotoso, W. Friesen, C. Fairbridge, Y. Shi, S. Ng, Solid transformation of zeolite NaA to sodalite, Microporous and Mesoporous Materials. 130 (2010) 303–308. https://doi.org/10.1016/j.micromeso.2009.11.025.
[33] M. Esaifan, L.N. Warr, G. Grathoff, T. Meyer, M.-T. Schafmeister, A. Kruth, H. Testrich, Synthesis of Hydroxy-Sodalite/Cancrinite Zeolites from Calcite-Bearing Kaolin for the Removal of Heavy Metal Ions in Aqueous Media, Minerals. 9 (2019) 484. https://doi.org/10.3390/min9080484.
[34] M. Dumańska-Słowik, A. Pieczka, W. Heflik, M. Sikorska, Cancrinite from nepheline syenite (mariupolite) of the Oktiabrski massif, SE Ukraine, and its growth history, Spectrochimica Acta Part A: Molecular and Biomolecular Spectroscopy. 157 (2016) 211–219. https://doi.org/10.1016/j.saa.2016.01.007.
[35] S. Khajavi, S. Sartipi, J. Gascon, J.C. Jansen, F. Kapteijn, Thermostability of hydroxy sodalite in view of membrane applications, Microporous and Mesoporous Materials. 132 (2010) 510–517. https://doi.org/10.1016/j.micromeso.2010.03.035.
[36] D.J. Schipper, T.W. Lathouwers, C.Z. Doorn, Thermal Decomposition of Sodalites, J American Ceramic Society. 56 (1973) 523–525. https://doi.org/10.1111/j.1151-2916.1973.tb12402.x.

[37] Z.D. Sharp, G.R. Helffrich, S.R. Bohlen, E.J. Essene, The stability of sodalite in the system $NaAlSiO_4$-NaCl, Geochimica et Cosmochimica Acta. 53 (1989) 1943–1954.